Acute myeloid leukemia shapes the bone marrow stromal niche *in vivo*

Emerging evidence suggests that acute myeloid leukemia (AML) remodels the bone marrow (BM) niche into a leukemia-permissive microenvironment, while suppressing normal hematopoiesis.[1] The influence of AML on bone tissue architecture and osteogenic cell differentiation has been documented in murine models, however, the impact of patient-derived AML cells on human BM stromal cells (BMSC) has only been investigated using conventional *in vitro* approaches. We assessed the differentiation potential of AML-derived BMSC using two *in vivo* models that recapitulate the complex organization of the human hematopoietic niche. We found that BMSC derived from pediatric AML patients: i) exhibit a reduced mature bone formation, ii) develop an osteoprogenitor-rich niche, iii) generate bone/BM organoids with a higher adipocytic differentiation, and iiii) support the formation of osteoclasts in a similar proportion to normal donor controls. All these aspects may contribute to the inhibition of normal hematopoietic stem and progenitor cell development and propagate selective blast cell survival and expansion.

AML is a heterogeneous disorder characterized by the clonal proliferation of blasts in the BM. Leukemic cells compete with normal hematopoietic stem cells for niche occupation and this results in alterations of the BM microenvironment and the generation of a "leukemic niche" that selectively supports the malignant clone.[1] AML-induced changes in the BM microenvironment have been confirmed in multiple *in vitro* and *in vivo* studies. Murine AML models have shown several alterations in the BM niche components (e.g., osteo-progenitors and osteoblasts) positively correlated with leukemogenesis.[2,3] Similarly, a decrease in osteoblast number has been observed in the BM of AML patients together with reduced osteocalcin serum levels.[4] Moreover, studies have also reported that BMSC, one of the main cellular components of the hematopoietic niche, derived from AML patients exhibit a number of molecular and functional alterations, such as translocations, gene expression modifications, reduced clonogenic potential, decreased proliferation, higher senescence, impaired *in vitro* adipogenic and osteogenic differentiation, increased support of leukemia growth, and imbalanced regulation of endogenous hematopoiesis.[5-7] By contrast, other studies have reported that AML-BMSC display normal morphology and differentiation properties.[8]

The humanized models are currently the only experimental system to reproduce an *in vivo* three-dimensional structure of the human BM niche, despite the limitations related to the potential interference of other components of recipient origins.[9] Several *in vivo* models have been described using normal or genetically modified human BMSC to generate a humanized BM niche that enables robust AML cell engraftment and allows evaluation of factors critical for the development/progression of leukemic cells within the niche.[9,10] The aim of our work was to evaluate if AML-BMSC have undergone significant changes in their capability to form bone and a BM niche after exposure to patient leukemia in the BM.

We isolated and expanded *in vitro* BMSC from the BM of newly diagnosed pediatric AML patients (AML-BMSC) and healthy donors (HD-BMSC). Patients and healthy controls were age-matched. BMSC donor characteristics are summarized in the *Online Supplementary Table S1*. BMSC from both sources displayed a spindle-shaped, elongated morphology and formed discrete fibroblast colony-forming units with no differences in colony-forming efficiency (CFE) and in the number of cumulative population doublings (CPD) (Figure 1A-C). Similarly, BMSC derived from both sources revealed an identical *in vitro* immunophenotype consistent with standard criteria (Figure 1D). As a few studies have described impaired hematopoietic support capacities of AML-derived BMSC,[6] we investigated several cell-bound as well as secreted factors governing the hematopoiesis within the niche. We found significantly diminished mRNA levels of Kit-ligand (*KITLG*), while other hematopoiesis regulatory molecules such as VCAM1, Angiopoietin-1, CXCL12, and Jagged1 were unaffected (Figure 1E). We then evaluated the *in vitro* skeletogenic potential of AML-BMSC *versus* HD-BMSC by performing quantitative gene expression of known osteogenic and chondrogenic genes at baseline in monolayer cultures without the addition of any inducing factors. We found a similar expression in both AML-BMSC and HD-BMSC, except for *SP7/Osterix* levels which were significantly reduced in AML-BMSC (Figure 1F). *In vitro* adipogenic, osteogenic, and chondrogenic differentiation assays showed normal tri-lineage differentiation potential for AML-BMSC population as proven by morphology, cytochemical staining, and up-regulation of mRNA levels of tissue-specific markers (Figure 1G).

The previously published data on *in vitro* AML-BMSC functional properties, mainly conducted using adult patient cohort samples, are contradictory. One of the reasons for such heterogeneity could be related to the age of patients. AML in young and adult patients should be considered differently since the biological and molecular characteristics of leukemic cells are different. In previous studies that included also pediatric cases, the reduction of adipogenic and osteogenic differentiation potential was correlated with AML characteristics at diagnosis and not to the patients' age.[8,11] In contrast, as our results confirm, the differential proliferative capacity of AML-BMSC is related to the age of the patients, with older patient samples displaying a reduction in proliferative ability when compared to younger patient samples.

The conventional *in vitro* differentiation assays are partially predictive of the *in vivo* physiologic functions of BMSC as these cultures leverage artificial inducing differentiation factors that do not necessarily reflect the intrinsic physiological potential of the cells.[12] Therefore, in order to accurately assess the *in vivo* functional properties of AML-BMSC in a physiologic environment we used two distinct heterotopic transplantation models to assess the osteogenic activity as well as the capacity to establish a complete hematopoietic niche, respectively. The first assay, which allows evaluation of the BMSC differentiation capacity into osteoblasts based on the formation of histologically-provable bone, was performed by implanting AML-BMSC or HD-BMSC loaded on an osteoconductive hydroxyapatite/tricalcium phosphate carrier in subcutaneous tissues of immunocompromised SCID/beige mice.[13] Histological analysis of the transplants harvested at 8 weeks revealed bone deposition in both groups (Figure 2A-B). Immunostaining of sections with an anti-osterix antibody showed the presence in AML-derived ossicles of osterix-expressing osteoprogenitor cells accompanied by osterix-positive osteocytes (Figure 2C, top panels). Immunostaining with an anti-osteocalcin antibody, a marker for mature osteoblasts, revealed a virtual absence of positive cells along the bone surfaces in the AML-derived implants and osteocyte immunoreactivity in both AML- and HD-derived

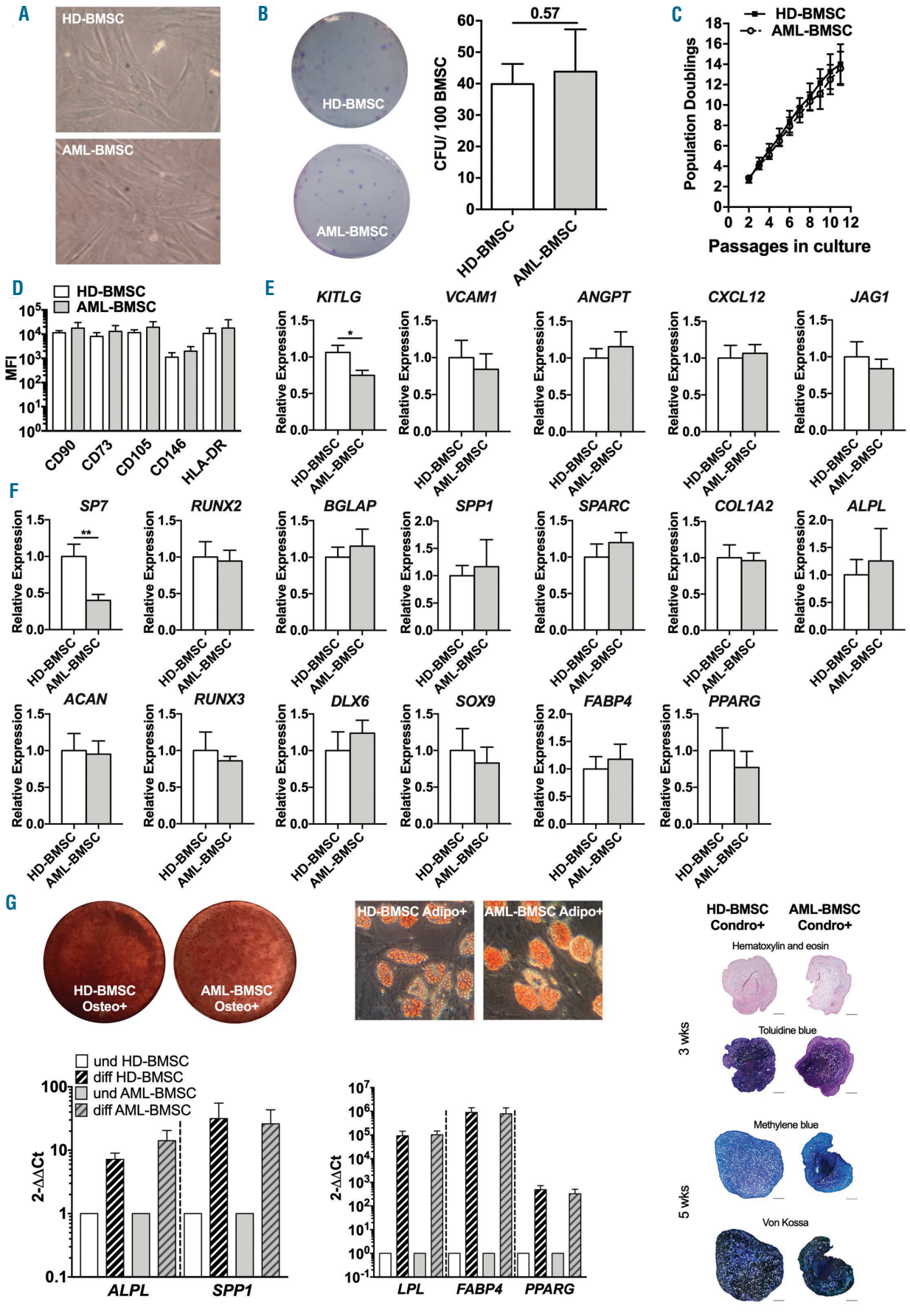
A
HD-BMSC
AML-BMSC
B
HD-BMSC
AML-BMSC
0.57
CFU/ 100 BMSC
HD-BMSC
AML-BMSC
C
HD-BMSC
AML-BMSC
Population Doublings
Passages in culture
D
HD-BMSC
AML-BMSC
MFI
CD90
CD73
CD105
CD146
HLA-DR
E
KITLG
VCAM1
ANGPT
CXCL12
JAG1
Relative Expression
F
SP7
RUNX2
BGLAP
SPP1
SPARC
COL1A2
ALPL
ACAN
RUNX3
DLX6
SOX9
FABP4
PPARG
G
HD-BMSC Osteo+
AML-BMSC Osteo+
HD-BMSC Adipo+
AML-BMSC Adipo+
HD-BMSC Condro+
AML-BMSC Condro+
Hematoxylin and eosin
Toluidine blue
Methylene blue
Von Kossa
3 wks
5 wks
und HD-BMSC
diff HD-BMSC
und AML-BMSC
diff AML-BMSC
2-ΔΔCt
ALPL
SPP1
LPL
FABP4
PPARG

(previous page) **Figure 1. *In vitro* characterization of bone marrow stromal cells derived from bone marrow of pediatric acute myeloid leukemia patients and healthy donors.** (A) Phase-contrast images depicting spindle-shaped morphology of bone marrow stromal cells (BMSC) derived from pediatric acute myeloid leukemia (AML) patients and healthy donors (HD). Magnification 40x. (B) Colony forming unit (CFU-F) potential of AML- and HD-BMSC. Representative images of AML and HD CFU-F are shown in the left panel. Bar charts show mean ± standard deviation (SD) of CFU-F numbers normalized to 100 plated BMSC derived from AML (gray bar) vs. HD (white bar). (C) Proliferation measured as cumulative population doubling at each passage for AML-BMSC and HD-BMSC cultures. Bars show mean ± SD. (D) Expression of surface markers CD90, CD73, CD105, CD146, and HLA-DR on AML-BMSC and HD-BMSC at passage three. Bars represent mean ± SD of mean fluorescence intensity (MFI) values. (E) Quantitative RT-PCR-based analysis of the baseline expression of hematopoietic niche regulatory genes in AML-BMSC and HD-BMSC populations. KIT ligand (*KITLG*), vascular cell adhesion molecule 1 (*VCAM1*), angiopoietin 1 *(ANGPT1*), *CXCL12*, and Jagged1 (*JAG1*) expression was analyzed in BMSC derived from AML (n=8, independent donors) compared with HD (n=8 independent donors). Expression levels for each gene compared with the GAPDH housekeeping gene are shown as mean ± standard error of the mean (SEM). (F) Quantitative RT–PCR–based analysis of the baseline expression of transcription factors and lineage-specific genes associated with bone, cartilage, and adipose tissue formation in AML-BMSC and HD-BMSC populations. Osterix (*SP7*), runt-related transcription factor 2 (*RUNX2*), osteocalcin (*BGLAP*), osteopontin (*SPP1*), osteonectin (*SPARC*), type I collagen α2 chain (*COL1A2*), alkaline phosphatase (*ALPL*), aggrecan (*ACAN*), *RUNX3*, distal-less homeobox 6 (*DLX6*), SRY-box 9 (*SOX9*), fatty acid-binding protein 4 (*FABP4*), and peroxisome proliferator-activated receptor γ (*PPARG*) expression was analyzed in at least four independent donors. Expression levels for each gene compared with the *GAPDH* housekeeping gene are shown as mean ± SEM. (G) Tri-lineage *in vitro* differentiation of AML-BMSC and HD-BMSC. BMSC were induced to differentiate along osteogenic, adipogenic, and chondrogenic lineage *in vitro* according to standard protocols. After 21 days of osteogenic induction, cells were stained with Alizarin Red for visualization of Ca^{2+} accumulation (left panel). Adipogenic differentiation capacity was visualized after 21 days of induction by staining lipid droplets with Oil Red O (middle panel). The osteogenic and adipogenic differentiation was further verified by quantitative RT-PCR–based analysis for the expression of lineages markers (for *osteogenesis*: *ALPL* and *SPP1*; for adipogenesis: lipoprotein lipase (*LPL*), *FABP4*, and *PPARG*). *GAPDH* was used as reference housekeeping gene. Three-dimensional chondrogenic differentiation assay was used for evaluation of chondrogenic differentiation potential (right panel). After 21 days of induction, sections from cartilaginous pellets were stained with hematoxylin/eosin and Toluidine blue (top panels). Presence of chondrocytes within lacunae and of proteoglycans within cartilaginous matrix (Toluidine blue positive) reveal chondrogenic differentiation. Chondrogenesis was prolonged for an additional 2 weeks to obtain hypertrophic cartilage stained by methylene blue (bottom panels). Calcium deposition was stained in black using von Kossa. Scale bars represent 200 μm. For interindividual comparison the two-sided unpaired Students' *t*-test was employed. Statistical significance was established at $P \leq 0.05$. *$P \leq 0.05$, **$P \leq 0.01$. und: undifferentiated; diff: differentiated; wks: weeks.

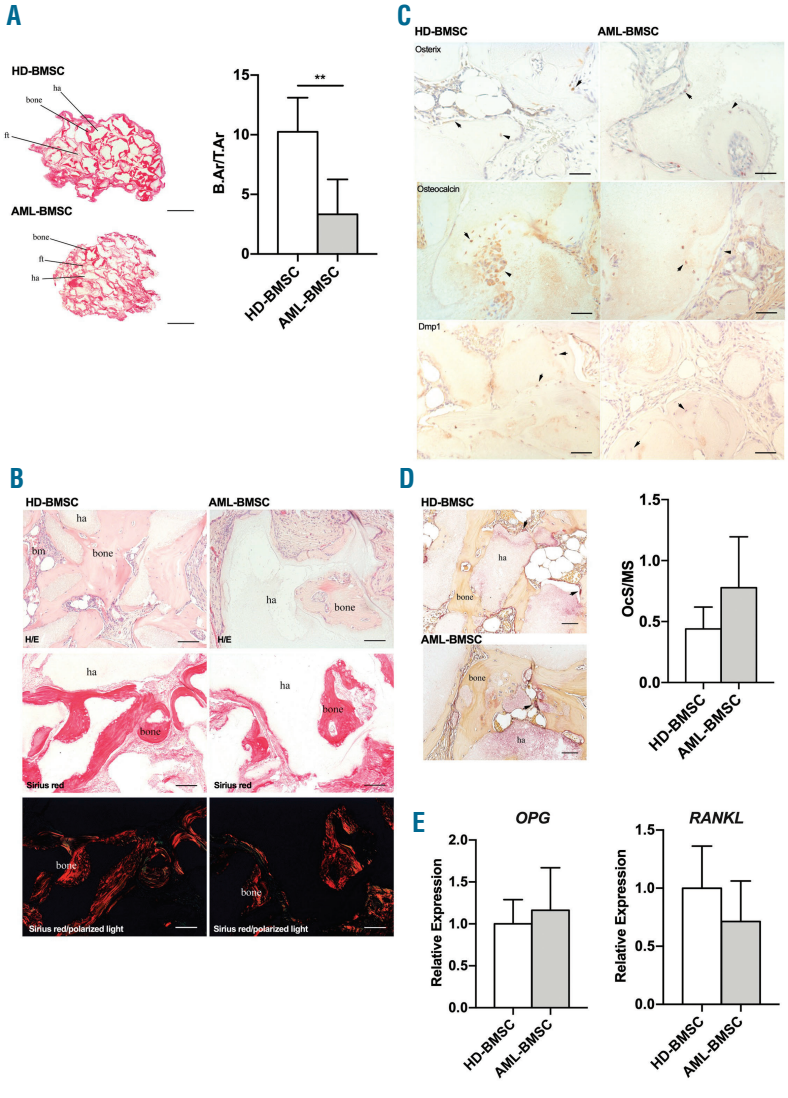

Figure 2. Altered *in vivo* osteogenic potential of acute myeloid leukemia bone marrow stromal cells. (A) In order to study osteogenesis *in vivo* a heterotopic transplantation assay was performed. $2x10^6$ acute myeloid leukemia bone marrow stromal cells (AML-BMSC) or healthy donor BMSC (HD-BMSC) were loaded onto a hydroxyapatite/tricalcium phosphate carrier and transplanted subcutaneously in the back of the immunocompromised SCID/beige mice. After 8 weeks, the grafts were harvested. Whole-mount Sirius red stained sections of HD-BMSC and AML-BMSC derived grafts (left panel). Scale bars represent 1 mm. Analysis of bone area/tissue area (B.Ar/T.Ar) by histomorphometry (right panel). Columns show the mean ± standard deviation of AML (n=7 grafts from three independent donors) and HD (n=6 grafts from two independent donors). **$P \leq 0.01$. (B) Histological analysis of hematoxylin/eosin (H/E) stained sections (top panel) of both AML-BMSC and HD-BMSC heterotopic transplants revealed new bone formation along the hydroxyapatite carrier, and marrow cavities with adipocytes and host hematopoietic cells. Transmitted (central panel) and polarized- (bottom panel) light view of the same microscopic field stained with Sirius red highlighted the newly formed bone and its lamellar structure. Scale bars represent 100 μm. (C) Representative images of immunohistochemical staining for osterix (upper panel), osteocalcin (central panel), and DMP1 (bottom panel). Osterix positive osteoprogenitor cells and osteocytes (arrow and arrowhead, respectively) are detected in AML-derived samples. Conversely, in AML-BMSC derived grafts osteocalcin expression is closely restricted to osteocytes, as opposed to HD-BMSC transplants in which osteocalcin expression is detected either in osteoblasts and osteocytes (arrow and arrowhead, respectively). Moreover, osteocytes in AML-BMSC derived grafts are completely negative for DMP1, contrary to what was observed in HD-derived samples (arrowhead). Scale bars represent 50 μm. (D) Representative images of sections stained for the osteoclastic marker TRAP (left panel). Scale bars represent 50 μm. Quantification of the mineralized surface (bone surface plus scaffold surface) lined by TRAP+ multinucleated osteoclasts (OcS/MS, right panel). Columns show the mean ± standard deviation of AML (n=6 grafts from two independent donors) and HD (n=4 grafts from two independent donors). (E) Quantitative RT-PCR–based analysis of the baseline expression of osteoclasts differentiation regulators osteoprotegerin (*OPG*) and receptor activator of nuclear factor-κ B ligand (*RANKL*) in BMSC derived from AML (n=8 independent donors) compared with HD (n=8 independent donors). Expression levels compared with the GAPDH housekeeping gene is shown as mean ± standard error of the mean.

implants (Figure 2C, central panels). Moreover, immunostaining with dentin matrix acid phosphoprotein 1 (DMP1), a marker of mature osteocytes, revealed the presence of DMP1-negative osteocytes in AML-BMSC derived grafts, which differed from HD-BMSC transplants (Figure 2C, bottom panels).

In addition, histomorphometric analysis displayed a significantly reduced amount of bone tissue in AML-derived implants (bone area/tissue area [B.Ar/T.Ar] %; AML-derived *vs.* HD-derived implants: 3.33±1.11 *vs.* 10.24±1.28, *P*=0.002) (Figure 2A, right panel). Moreover, no changes were detected in the mineralized surface cov-

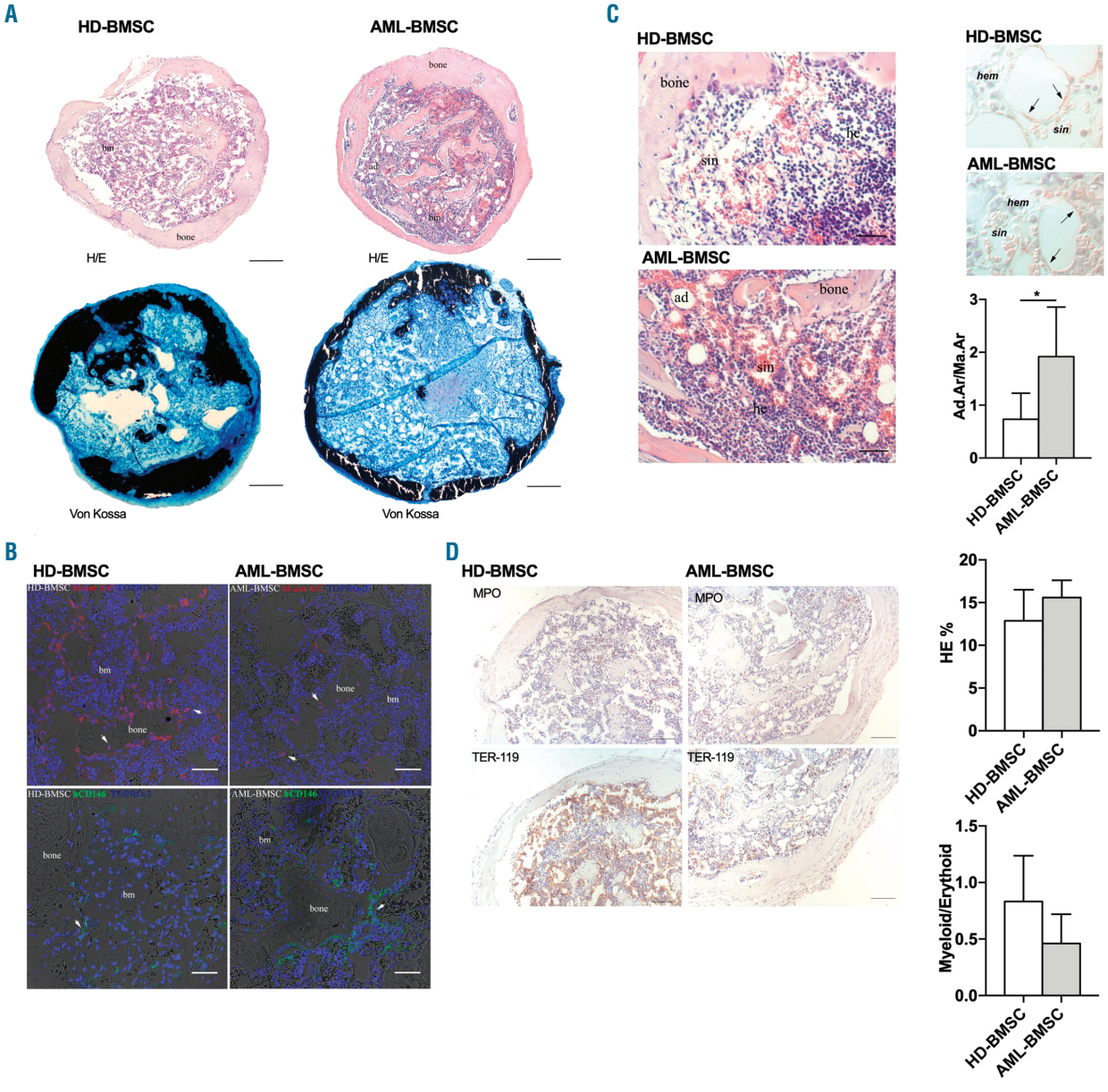

Figure 3. Altered *in vivo* bone marrow stromal niche formation by acute myeloid leukemia bone marrow stromal cells. (A) In order to study the capacity to recapitulate the hemopoietic niche *in vivo*, acute myeloid leukemia bone marrow stromal cells (AML-BMSC) or healthy donor BMSC (HD-BMSC) were cultured for 3 weeks as micro-masses in chondrogenic differentiation medium and then unmineralized pellets were transplanted subcutaneously into immunocompromised NSG mice. Eight weeks after transplantation, the bone/BM organoids were harvested. Representative images of AML- and HD-derived grafts are shown. Hematoxylin/eosin (H/E) stain (upper panel) revealed the presence, in both AML- and HD-ossicles, of a bony cortex with an inner marrow cavity containing murine hematopoietic cells. Undecalcified von Kossa/methylene blue stained sections (bottom panel) evidenced comparable levels of bone mineralization in AML- and HD-derived ossicles. Scale bars represent 200 μm. (B) Confocal fluorescence images confirming the human origin of the heterotopic ossicle. The human specific LaminA/C is detected in the nuclear membrane of osteocytes (arrows) and spread marrow cells (top panel). Bottom panel shows representative images of immunofluorescence staining for hCD146 of BMSC in association with vessels walls. Cell nuclei were stained with Topro-3 iodide. Scale bars represent 50 μm. (C) Details of marrow tissues in AML- and HD-derived ossicles are shown (H/E stain, left panel). Trabecular bone, hematopoiesis (he), adipocytes (ad) and sinusoids (sin) are observable (scale bars: 50 μm). Adipocytes were stained for perilipin (right top panel). Quantitative analysis of BM fraction occupied by adipocytes within bone/BM organoids (adipocyte area/marrow area [Ad.Ar/Ma.Ar], right low panel) demonstrated that *in vivo* adipogenic differentiation was increased in AML-BMSC. Columns shows the mean ± standard deviation (SD) of AML (n=5 grafts from three independent donors) and HD (n=5 grafts from two independent donor). (D) Quantification and characterization of hematopoietic tissue in the intertrabecular space within the ossicles. Evaluation of the presence of myeloid (MPO+) and erythroid cells (Ter-119+) within murine hematopoietic foci of AML- and HD-ossicles (left panel). Scale bars represent 100 μm. Quantification of total hematopoietic tissue in bone/BM organoids (right top panel). Quantification of myeloid/erythroid ratio in organoids (right low panel). Columns show the mean ± standard deviation of AML (n=4 grafts from three independent donors) and HD (n=2 grafts from two independent donor). bm: bone marrow.

ered by multinucleated tartrate-resistant acid phosphatase (TRAP) positive osteoclasts (OcS/MS %) (Figure 2D). Mirroring this histologic finding, gene expression of the osteoclast differentiation regulators *RANKL* and *OPG* evaluated by quantitative RT-PCR in basal BMSC from both sources was similar (Figure 2E). These data indicate an impaired osteogenic potential of AML-derived BMSC, suggesting that leukemia cells can interfere with the maturation of osteoblast precursors which in turn results in reduced bone formation in the absence of changes in osteoclastic activity. It cannot be excluded that the osteogenic differentiation blockade may be a result of epigenetic changes in AML-BMSC affecting the genes involved in osteogenic cell development, such as PTX2 and TBX15 transcription factors.[7] Our finding is consistent with previous reports demonstrating perturbation of the osteogenic niche in AML mouse models and in AML and myelodysplastic patients.[2,4,14] Specifically, studies have shown that AML leads to the accumulation of osterix-expressing osteoblast-primed cells in murine BM.[15]

We next assessed the ability of AML-BMSC to form a BM cavity and a functional stromal niche using a model consisting in *in vivo* implantation of cartilage pellets followed by the progressive substitution of cartilage by marrow through a process we named "endochondral myelogenesis".[16] AML-BMSC and HD-BMSC were grown as unmineralized pellets in chondrogenic differentiation medium and then implanted subcutaneously into NSG mice. After 8 weeks, implanted chondroid pellets were replaced by a BM hematopoietic microenvironment composed of human-derived skeletal tissues (bone, cartilage, fat, and perivascular cells), as confirmed by staining with human-specific LaminA/C, and mouse-derived hematopoietic cells (Figure 3A-B). Furthermore, in AML-ossicles we detected the presence of human CD146-positive stromal cells associated with the vessel wall (Figure 3B). Interestingly, AML-BMSC derived ossicles contained a significantly increased fraction occupied by adipocytes, when compared to HD-BMSC transplants (adipocyte area/marrow area [Ad.Ar/Ma.Ar] %; AML-derived *vs.* HD-derived implants: 1.92±0.42 *vs.* 0.73±0.22; P=0.037) (Figure 3C). Our results agree with other reports showing that BM-stromal progenitors from AML mice have an increased adipogenic differentiation ability.[3] Moreover, Lu *et al*. found that marrow of AML patients in remission had less adipocyte content than cases from non-remission marrows as compared with diagnostic marrows.[17]

Lastly, the amount of hematopoietic tissue and the myeloid/erythroid (MPO+/TER-119+) ratio in normal and patient-derived ossicles were similar (Figure 3D).

In conclusion, we have demonstrated using *in vivo* physiologic models that AML-BMSC function is significantly altered in mature bone formation and niche composition. As demonstrated by these *in vivo* transplantation assays, BM-stromal progenitors from pediatric AML patients, even when removed from their pathological environment, show an intrinsically abnormal differentiation pattern with altered osteogenesis and increased adipogenic potential, which is not easily detectable by canonical *in vitro* assays. This suggests an instructive role of leukemic cells on the BM microenvironment that can contribute to the generation of a supportive niche for leukemic cells themselves. As our study leveraged *in vivo* models that appropriately reproduce the human BM niche, our data may have an important clinical relevance. Understanding the unique characteristics of the AML osteogenic niche represents a critical step towards unraveling the mechanisms underlying osteogenic niche-mediated support of AML cells and leukemic progression. Our data suggests the possibility to target stage-specific cells of the osteogenic lineage to normalize the hostile BM niche and suppress AML cell development and proliferation with an ultimate goal of inducing deep remissions and controlling long-term disease.

Alice Pievani,[1] Samantha Donsante,[2*] Chiara Tomasoni,[1] Alessandro Corsi,[2] Francesco Dazzi,[3] Andrea Biondi,[1,4] Mara Riminucci[2] and Marta Serafini[1]*

**AP and SD contributed equally as co-first authors*

[1]Centro Ricerca M. Tettamanti, Department of Pediatrics, University of Milano-Bicocca, Monza, Italy; [2]Department of Molecular Medicine, Sapienza University, Rome, Italy; [3]Department of Hemato-Oncology, Rayne Institute, King's College London, London, UK and [4]Department of Pediatrics, Fondazione MBBM/San Gerardo Hospital, Monza, Italy

Correspondence: MARTA SERAFINI - serafinim72@gmail.com

doi:10.3324/haematol.2020.247205

Disclosures: no conflicts of interest to disclose.

Contributions: AP collected and analyzed the data and wrote the manuscript; SD performed in vivo experiments, analyzed the data, and contributed to the manuscript writing; CT performed in vitro experiments; AC and MR interpreted the data and critically revised the manuscript, FD and AB critically revised the manuscript; MS supervised the research and wrote the manuscript.

Acknowledgments: the authors would like to thank Fondazione Matilde Tettamanti, Comitato Maria Letizia Verga, Fondazione MBBM, Associazione SKO Arianna Amore Onlus for their generous support.

Funding: this work was partially supported by AIRC-5 per mille 2018-21147 to AB, and AIRC-2015-17248 to MS.

References

1. Lane SW, Scadden DT, Gilliland DG. The leukemic stem cell niche: current concepts and therapeutic opportunities. Blood. 2009; 114(6):1150-1157.
2. Frisch BJ, Ashton JM, Xing L, Becker MW, Jordan CT, Calvi LM. Functional inhibition of osteoblastic cells in an in vivo mouse model of myeloid leukemia. Blood. 2012;119(2):540-550.
3. Kumar B, Garcia M, Weng L, et al. Acute myeloid leukemia transforms the bone marrow niche into a leukemia-permissive microenvironment through exosome secretion. Leukemia. 2018;32(3):575-587.
4. Krevvata M, Silva BC, Manavalan JS, et al. Inhibition of leukemia cell engraftment and disease progression in mice by osteoblasts. Blood. 2014;124(18):2834-2846.
5. Blau O, Baldus CD, Hofmann WK, et al. Mesenchymal stromal cells of myelodysplastic syndrome and acute myeloid leukemia patients have distinct genetic abnormalities compared with leukemic blasts. Blood. 2011;118(20):5583-5592.
6. Kim JA, Shim JS, Lee GY, et al. Microenvironmental remodeling as a parameter and prognostic factor of heterogeneous leukemogenesis in acute myelogenous leukemia. Cancer Res. 2015;75(11):2222-2231.
7. Geyh S, Rodriguez-Paredes M, Jager P, et al. Functional inhibition of mesenchymal stromal cells in acute myeloid leukemia. Leukemia. 2016;30(3):683-691.
8. Desbourdes L, Javary J, Charbonnier T, et al. Alteration analysis of bone marrow mesenchymal stromal cells from de novo acute myeloid leukemia patients at diagnosis. Stem Cells Dev. 2017;26(10):709-722.
9. Abarrategi A, Mian SA, Passaro D, Rouault-Pierre K, Grey W, Bonnet D. Modeling the human bone marrow niche in mice: from host bone marrow engraftment to bioengineering approaches. J Exp Med. 2018;215(3):729-743.
10. Le PM, Andreeff M, Battula VL. Osteogenic niche in the regulation of normal hematopoiesis and leukemogenesis. Haematologica. 2018;103(12):1945-1955.
11. Diaz de la Guardia R, Lopez-Millan B, Lavoie JR, et al. Detailed characterization of mesenchymal stem/stromal cells from a large cohort of AML patients demonstrates a definitive link to treatment outcomes. Stem Cell Reports. 2017;8(6):1573-1586.

12. Gimble JM, Guilak F, Nuttall ME, Sathishkumar S, Vidal M, Bunnell BA. In vitro differentiation potential of pesenchymal stem cells. Transfus Med Hemother. 2008;35(3):228-238.
13. Sacchetti B, Funari A, Michienzi S, et al. Self-renewing osteoprogenitors in bone marrow sinusoids can organize a hematopoietic microenvironment. Cell. 2007;131(2):324-336.
14. Battula VL, Le PM, Sun JC, et al. AML-induced osteogenic differentiation in mesenchymal stromal cells supports leukemia growth. JCI Insight. 2017;2(13):e90036.
15. Hanoun M, Zhang D, Mizoguchi T, et al. Acute myelogenous leukemia-induced sympathetic neuropathy promotes malignancy in an altered hematopoietic stem cell niche. Cell Stem Cell. 2014;15(3):365-375.
16. Serafini M, Sacchetti B, Pievani A, et al. Establishment of bone marrow and hematopoietic niches in vivo by reversion of chondrocyte differentiation of human bone marrow stromal cells. Stem Cell Res. 2014;12(3):659-672.
17. Lu W, Weng W, Zhu Q, et al. Small bone marrow adipocytes predict poor prognosis in acute myeloid leukemia. Haematologica. 2018;103(1):e21-e24.